Targeted mutagenesis in *Nicotiana tabacum ADF* gene using shockwave-mediated ribonucleoprotein delivery increases osmotic stress tolerance

Sruthy Maria Augustine (Sruthy.Augustina@agrar.uni-giessen.de)
Justus Liebig University, Giessen

Anoop Vadakan Cherian
Fraunhofer IME

Kerstin Seiling
RWTH Aachen University

Stefano Di Fiore
Fraunhofer IME

Nicole Raven
Fraunhofer IME

Ulrich Commandeur
RWTH Aachen University

Stefan Schillberg
Fraunhofer Institute for Molecular Biology and Applied Ecology IME https://orcid.org/0000-0002-1896-4575

Research Article

Keywords: Nicotiana tabacum, shock waves, Ribonucleoprotein complex, genome-edited plants, actin, interlocking marginal lobes

Posted Date: July 7th, 2021

DOI: https://doi.org/10.21203/rs.3.rs-98241/v2

Abstract

DNA-free genome editing involves the direct introduction of ribonucleoprotein (RNP) complexes into cells, but this strategy has rarely been successful in plants. In the present study, we describe a new technique for the introduction of RNPs into plant cells involving the generation of cavitation bubbles using a pulsed laser. The resulting shockwave achieves the efficient transfection of walled cells in tissue explants by creating transient membrane pores. RNP-containing cells were rapidly identified by fluorescence microscopy, followed by regeneration and the screening of mutant plants by high-resolution melt analysis. We used this technique in *Nicotiana tabacum* to target the endogenous *PHYTOENE DESATURASE* (*PDS*) and *ACTIN DEPOLYMERIZING FACTOR* (*ADF)* genes. Genome-edited plants were produced with an efficiency of 35.2% for *PDS* and 16.5% for *ADF*. Further we evaluated the physiological, cellular and molecular effects of *ADF* mutations in T2 mutant plants under drought and salinity stress. The results suggest that *ADF* acts as a key regulator of osmotic stress tolerance in plants.

Introduction

Genome editing in plants is widely used for the functional analysis of genes and the development of improved crop varieties. The CRISPR/Cas9 system is the most popular genome-editing tool because it is simple and adaptable, especially for the simultaneous mutation of multiple genes (Jeffry et al. 2014; Schiml et al. 2016; Wang et al. 2016). CRISPR/Cas9 has therefore been used to manipulate many traits of agricultural significance (Zhou et al. 2015; Wang et al. 2016; Zhang et al. 2017; Ortigosa et al. 2018; Yao et al., 2018; Kawal. 2019; Zhang et al. 2020). However, the major limitation of CRISPR/Cas9 technology in plant biology is the need for stable transformation, which involves the introduction of an expression cassette providing the Cas9 nuclease, the guide RNA (gRNA), and a selection marker (Altpeter et al. 2016; Sedeek et al. 2019). The hostility towards genetically-modified plants in some jurisdictions calls for DNA-free genome editing methods, in which RNPs containing the Cas9 nuclease and RNA components fulfilling the function of gRNA are first assembled in vitro and then introduced into plant cells using standard transfection procedures. The advantages of RNP-mediated genome editing include the prompt but transient activity of Cas9, reducing the frequency of off-target mutations, and the fact that the resulting genome-edited plants are considered transgene-free (Guha et al. 2017).

We have previously shown that RNP-mediated transient genome-editing targeting the tobacco *PDS* gene showed mutation when the RNP was delivered by particle bombardment, but the absence of a selection marker resulted in a laborious and time-consuming screening process and no stable transformants (Bortesi et al. 2017). Furthermore, particle bombardment causes severe cell damage and the efficiency of regeneration is therefore low (O'Brien et al. 2001; Thomas et al. 2001; O'Brien et al. 2011). PEG-mediated protoplast transfection is a gentler method for the delivery of CRISPR/Cas9 components (as DNA, RNA or RNPs) (Woo et al. 2015; Mickael et al. 2016; Sant'Ana et al. 2020), but the efficient regeneration of many plant species from protoplasts is not yet possible (Lin et al. 2018). DNA-free genome editing, therefore, remains challenging in species recalcitrant to transformation, such as wheat, sorghum and woody plants

(Li et al. 2016; Mao et al. 2019). A new method, gentle and compatible with intact plant cells, is required for the delivery of RNPs.

Shock waves induced by cavitation bubbles show great potential for the delivery of nucleic acids and proteins because they create transient pores in the plasma membrane, thus increasing its permeability (Tachibana et al. 1999; Maochen et al. 2018). Cavitation bubbles are usually induced by acoustic stimuli such as ultra-sonication, and the resulting shock waves can promote the uptake of DNA by plant cells (Miller et al. 2002). This non-invasive and chemical-free method has been used to transfect individual plant cells, protoplasts, plant cell suspension cultures, and intact tissue explants (Liu et al., 2006; Lin et al. 2018). Although the generation and oscillation of gas bubbles in liquid is usually achieved by acoustic cavitation (Leighton. 1995; Miller et al. 2002), shock waves can also be produced by a pulsed laser, an approach that has not yet been used for plants but was successful for the transfection of animal cells (Juhasz et al., 1994; Cherian et al. 2008). Based on these findings, we adapted the pulsed laser method for the transfection of intact plant cells with CRISPR/Cas9 RNPs.

The new pulsed laser technique has the potential to increase the efficiency of genome editing in a broad range of plant species that are able to regenerate from leaf cells and particularly from epidermal leaf cells. The rapid selection of RNP-containing cells was achieved by incorporating a labeled RNA detected by fluorescence microscopy. This was followed by regeneration and the screening of mutant plants by high-resolution melt analysis (HRMA). We targeted the endogenous *PHYTOENE DESATURASE* gene (*PDS*) because mutations generate an easy, detectable albino phenotype allowing the calculation of mutation efficiency. We also targeted the *ACTIN DEPOLYMERIZING FACTOR* (*ADF*) gene because mutations increase osmotic stress tolerance, allowing us to demonstrate the potential of our new method for the modification of agriculturally-relevant traits. Accordingly, we also evaluated the phenotype of *adf* mutant T2 plants under drought and salinity stress, providing insight into the role of the actin cytoskeleton in abiotic stress tolerance. This is the first report on the introduction of RNP into intact plant cells using cavitation-induced shock wave method and generation of osmotic stress-tolerant *adf* mutant plants.

Materials And Methods

2.1-Plant material, resequencing of target genes and gRNA design

Genomic DNA was extracted from wild-type tobacco plants (*Nicotiana tabacum* cv Petit Havana SR1) (3–4 weeks old, when the plants had reached the 2–3 leaf stage; Pospíšilová et al. 1998) using the NucleoSpin Plant II kit (Macherey-Nagel). The target regions of the selected *PDS* and *ADF* genes were amplified from genomic DNA using Q5 high-fidelity DNA polymerase (NEB). The PCR products were purified from agarose gels using the NucleoSpin gel and PCR clean-up kit (Macherey-Nagel) and sequenced using the Sanger method prior to gRNA design, using the primers listed in the Table S1. The gRNA sequences were designed using the Crispr RGEN Tools, Cas-Designer and CRISPR-P v2.0 online. The gRNA targeting the *PDS* gene was 5'-TTTTTTTGGAATATCAGGTTTGG-3' and the gRNA targeting the *ADF* gene was 5'-CTTGGAGCTGAAGAGGAAGAAGG-3'. BLAST analysis was used to identify any potential

off-targets in the crRNA sequences. To prepare RNP complexes, we used crRNA, tracrRNA labeled with ATTO-550 and high fidelity Cas9 (HiFi Cas9) synthesized by Integrated DNA Technologies. We used crRNA XT for all experiments, which has additional chemical modifications to optimize stability and performance.

2.2-Transfection mediated by cavitation bubble-induced shockwaves

Shockwaves were produced out of cavitation bubbles generated using a Mai Tai DeepSee Multiphoton pulsed laser (Spectra-Physics) coupled to an inverted TCS SP8 confocal microscope (Leica Microsystems). In order to standardize the transfection conditions, leaf discs (~10 × 5 mm) were placed in a microscopy-grade 35-mm Petri dish with a glass bottom (ibidi µ-dish) containing 20 µL 0.25 µg μL^{-1} *Discosoma striata* red fluorescent protein (DsRed) R2G mutant, expressed from pGJ1425 (MPI; Sack et al., 2015). For all experiments, the laser was set to 900 nm and the beam was focused 2–5 µm beneath the lowest epidermal cells of the leaf discs. The laser was used to irradiate a single focused region (six pulses over 1.29 s), creating a plasma that induced bubble formation. The resulting shockwaves transiently increased the permeability of the plasma membrane, allowing the uptake of DsRed into the leaf cells. Around 8-10 leaf pieces were transfected with DsRed. The transfection efficiency was calculated by using the equation:

% transfection efficiency = (number of cells contained DsRed/total number of cells per field) x 100

More details about the transfection setup and its implementation in another crop species (*Z. mays*) are given in Appendix S1 and Figures S1 and S2. The same laser setup was used for the delivery of RNPs, which were presented at the same concentration (0.25 µg μL^{-1}) as the DsRed protein. Approximately 30-35 leaf pieces were transfected with RNP and, in each leaf piece, 5-8 positions were treated by laser (Figure S2B). The detailed procedure for the preparation of RNP is given in Appendix S2.

2.3-Selection of cells transfected with RNPs

The leaf discs were visually inspected 48 h post-transfection under an Olympus X71 inverted fluorescence microscope equipped with appropriate filters for the detection of ATTO-550. Regions showing fluorescence were excised using pipette tips (1 mL and 200 µL capacity, shortened with scissors to achieve a radius of 0.1–0.3 cm) according to the area of RNP fluorescence. The selected regions containing the *PDS* or *ADF* RNPs were transferred to MS medium (4.4 g L^{-1} MS salts with vitamins (Duchefa), 20 g L^{-1} sucrose, 0.6 mg L^{-1} thiamine-HCl, 7 g L^{-1} agar, pH 5.8) with hormones (1 mg L^{-1} 6-BAP, 0.1 mg L^{-1} NAA) and incubated at 20–23°C. The regenerated tissue was subcultured onto plates with fresh medium every 2 weeks until shoots appeared (Pospíšilová et al. 1998). The plantlets were then transferred onto MS medium without hormones and incubated at 20–25°C with a 16-h photoperiod (7,000 lux) to induce root formation. Depending on the size of the selected and excised fluorescent leaf region, between 5-10 plants were typically obtained. The *adf* plants with roots were transferred to ED73 standard soil (Patzer) with 0–30% (v/v) sand and grown in the greenhouse with a 16-h photoperiod

(10,000 lux, plus sunlight) at 70–90% humidity. All plants were regenerated without selection reagents. All *pds* plants were analyzed at the 2–3-leaf stage on MS medium. Only the heterozygous mutants and wild-type plantlets developed roots, but these plants were not transferred to the greenhouse.

2.4-Genomic DNA extraction and HRMA

Genomic DNA was extracted from tobacco plants regenerated from discs using the Quick extract plant DNA extraction solution (Lucigen) according to the manufacturer's instructions. Leaf discs were collected from tobacco plants grown under sterile conditions at the 2–3-leaf stage. For initial screening, HRMA was carried out using a Quant studio3 Real-time PCR system with HRM software v3.1 (Thermo Fisher Scientific). Each 20-μL reaction contained 10 μL of MeltDoctor HRM master mix (Thermo Fisher Scientific), 0.25 μM of each primer and 50 ng genomic DNA. The melt curve analysis program included PCR amplification followed by melt analysis. For the *PDS* gene, the following conditions were used: PCR stage, 95°C for 10 min, followed by 40 cycles of 95°C for 15 s, 52°C for 1 min, and 72°C for 1 min; melt curve stage, 95°C for 15 s (1.6°C/s), 60°C for 1 min (1.6°C/s) and 95°C for 15 s (0.1°C/s). For the *ADF* gene, the following conditions were used: PCR stage, 95°C for 10 min, followed by 40 cycles of 95°C for 15 s, 57°C for 1 min, and 72°C for 1 min; melt curve stage, 95°C for 15 s (1.6°C/s), 60°C for 1 min (1.6°C/s), and 95°C for 15 s (0.1°C/s). All amplicons were 100–150 bp in length, and the site-specific primers listed in Table S2 were designed using Primer 3 software.

2.5-Sanger sequencing and analysis

The target sites for genome editing were amplified by PCR using 50 ng genomic DNA, 1.5 mM dNTPs, 0.25 μM of each primer, and one unit of Q5 high fidelity DNA polymerase for each 20-μL reaction. For the *PDS* gene, the reaction was heated to 98°C for 30 s, followed by 30 cycles of 98°C for 10 s, 56°C for 30 s, and 72°C for 30 s, then a final extension step at 72°C for 7 min before cooling to 4°C. For the *ADF* gene, the reaction was heated to 98°C for 30 s, followed by 30 cycles of 98°C for 10 s, 53°C for 30 s, and 72°C for 30 s, then a final extension step at 72°C for 7 min before cooling to 4°C. The PCR products were purified from agarose gels using the NucleoSpin gel and PCR clean-up kit and sequenced using the Sanger method on a 3730 DNA analyzer (Applied Biosystems). The primers used for Sanger sequencing are listed in Table S3.

The sequencing data were analyzed using CodonCode Aligner (CodonCode Corporation) and Clone Manager v9 Professional (Scientific & Educational Software, Denvar) by alignment with the wild-type reference sequence followed by the analysis of the chromatograms. For samples with biallelic mutations, the amplified PCR product was subcloned into the pTOPO vector from the TOPO TA Cloning Kit (Thermo Fisher Scientific) and plasmids from three or more independent clones were sequenced for confirmation.

2.6-Phalloidin staining and ImageJ analysis of *adf* mutant plants

Tobacco leaf discs (~10 × 5 mm) were stained with AlexaFluor 488 phalloidin as previously described (Kobayashi et al., 1997) with slight modifications (Opalski et al. 2005). The discs were fixed in 3.5% (v/v)

formaldehyde in phosphate-buffered saline (PBS, pH 7.4) at room temperature overnight. After washing in PBS, the discs were immersed in 0.5% (v/v) Triton X-100 in PBS (pH 7.4) at room temperature overnight. The discs were then washed three times in PBS and stained with 0.66 mM AlexaFluor 488 phalloidin in PBS (Thermo Fisher Scientific) at room temperature for 1 h in the dark before rinsing in PBS and mounting in PBS on glass slides. Actin microfilaments were observed under a Leica inverted TCS SP8 confocal microscope. Actin intensity in the Z projection of the apical membrane of the cells and the average intensity of the cell–cell junction were measured with the help of ImageJ software (Collins. 2007) for at least three independent plants of each mutant and wild-type line.

2.7-Cell membrane thermostability analysis

The cell membrane stability (CMS) test estimated the percentage of cell membrane injury as previously described (Martineau et al. 1979) and is an indicator of drought tolerance (Molaei et al. 2012). This parameter was studied in T_0 and T_2 mutant plants as well as wild-type plants. In the T_0 plants, we analyzed the membrane stability under normal irrigation. In the T_2 generation, the third fully-opened leaf was collected from mutant and wild-type plants on day 0 and 5 after the application of drought stress and 5 days after the reinstatement of normal irrigation. Leaf discs (0.5 cm diameter) weighing 200 mg were washed 3 x 2 min times with 20 mL distilled water. The leaf discs were then immersed in 20 mL distilled water in 2.5 cm × 15 cm tubes covered with aluminum foil and incubated at 60°C in a thermostatically controlled water bath for 20 min before cooling to 10°C for 12 h to allow the diffusion of electrolytes. An initial conductance reading was taken at 30°C using a conductivity meter, then the tubes were heated to 100°C for 20 min and a second conductance reading was taken after cooling to 30°C. Membrane injury % = $1 - ((1 - T_1/T_2)/(1 - C_1/C_2)) \times 100$, where T and C refer to the values for treatment and control samples, and the subscripts 1 and 2 denote the initial and final conductance readings, respectively.

2.8-Plant water status

The relative water content (RWC) of excised third leaves from mutant and wild-type plants at the 4–6-leaf stage was determined on day 0 and 5 after the induction of drought stress and 5 days after the reinstatement of normal irrigation. The RWC was calculated based on the fresh weight (FW), turgid weight (TW) and dry weight (DW) of 200-mg leaf samples. The FW was determined on a mass balance immediately after sample collection. The TW was determined after soaking the leaf discs in deionized water for 4 h at room temperature in a closed Petri dish and then blotting off any surface drops. The DW was determined after oven drying at 90°C for 72 h. The RWC was determined as previously described (Barrs & Weatherley 1962) using the following equation:

$$RWC = ((FW - DW) / (TW - DW)) \times 100$$

2.9-Gene expression analysis using the comparative CT method

Total RNA was isolated from leaf samples using Trizol reagent (Chomczynski & Mackey 1995) followed by treatment with DNase (Thermo Fisher Scientific). First-strand cDNAs were synthesized from total RNA using the Revert Aid first-strand cDNA synthesis kit and oligo (dT) primers (Thermo Fisher Scientific) with *β-ACTIN* as an internal control because its expression was not modified by drought stress. The expression of *β -ACTIN* was determined in both irrigated and drought-stressed samples to make sure that this gene did not respond to drought stress, so that it could be used as an internal control. Gene-specific primers designed using Primer Express v3 (Applied Biosystems) were then used for 40 cycles of specific amplification (Table S4). Each reaction comprised 12 µL Powerup SYBR green master mix (Thermo Fisher Scientific), 1 U *Taq* DNA polymerase and 10 pmol of each gene-specific primer and was carried out on a Step One real-time PCR system (Applied Biosystems). The CT values for both the target and internal control genes were used to quantify the transcripts by comparative CT normalization. All reactions were performed in triplicate, and the expression of the target gene was calculated using the formula $2^{-\Delta\Delta Ct}$ ((Ct gene of interest – Ct internal control) sample – (Ct gene of interest – Ct internal control) control; Livak & Schmittgen 2001). The $\Delta\Delta Ct$ values reflect the relative expression of the target gene following exposure to osmotic stress.

2.10-Seed germination assay

Thirteen T_1 seeds from each mutant line and wild-type controls were grown under identical controlled conditions in a greenhouse. To evaluate germination under salt stress conditions, the trays were irrigated daily with 0, 100, 200 or 300 mM NaCl for a period of 6 weeks. The number of seeds that germinated and the number of plants that survived were recorded at the end of 6 weeks. The experiment was carried out three times.

2.11-Statistical analysis

For statistical analysis of the data, ten independent mutant events with three replicates along with five wild-type plants with three replicates were used. Mean value, standard deviation and Student's *t*-test were evaluated using the XLSTAT 2013.5 program to analyze all the data to compare the mutant events and wild-type plants under normal and stress conditions. A P-value of ($P \leq 0.05$) was considered statistically significant.

Results

3.1-Fluorescent protein delivery into plant cells using a pulsed laser-induced shockwave

Unlike acoustic wave cavitation, pulsed laser cavitation can target shockwaves to a specific region of the sample. To fine-tune the transient increase in membrane permeability, we induced shock waves to transfect intact plant cells with a fluorescent protein (Figure 1A). We placed 10 x 5 mm intact leaf explants from 3-month-old tobacco plants cultivated under sterile conditions into an imaging-grade Petri dish with a glass bottom (Figure 1B) and added 20 µL of 0.25 µg μL^{-1} DsRed (Figure 1B). We focused a high-powered multiphoton laser 2–5 µm below the leaf sample and irradiated for approximately 8 s at a

laser power of ~2 W. This created a cavitation bubble-induced shockwave that successfully transfected the plant cells with DsRed (Video S1). We analyzed leaf explant cells before and after the laser pulse and observed DsRed emission in individual transfected cells by confocal microscopy (Figures 1C,C' and S2A). A schematic representation of the fluorescent tissue areas after transfection is given in Figure S2B. In average, 8-10 leaf explants were transfected with DsRed and 14.6% of the cells were transfected (Figure S2C). A 3D reconstruction of the transfected cells confirmed that DsRed was homogenously distributed in the cytoplasm (Figure 1C") and not merely attached to the cell surface. To demonstrate the applicability of the technique in another crop species, we introduced DsRed using pulsed laser-induced shock waves into 1-month-old *Z. mays* leaves. DsRed emission in transfected cells was analyzed by confocal microscopy before and after laser treatment (Figure S1).

3.2-RNP delivery into plant cells using a pulsed laser-induced shockwave and visual selection

Having established a working procedure, we then used the pulsed laser-induced shockwave method for the direct delivery of RNPs into the intact cells of tobacco leaf discs, which are much easier to prepare and handle than protoplasts or zygotes. We introduced a preassembled RNP comprising the HiFi Cas9 protein, crispr RNA (crRNA) and ATTO-550-labeled trans-activating crispr RNA (tracrRNA) targeting either the tobacco *PDS* or *ADF* genes. The fluorescent tracrRNA allowed the direct screening of transfected cells so that a selectable marker gene was unnecessary (Figure 2A'). The sample size and experimental setup were the same as described above for the transfection with DsRed (Figure 1A,B). In our observation, the ATTO-550 fluorescence started to become visible 24 h after laser treatment showing a maximum at 48 h post-transfection. According to the manufacturer, the RNP complex is active for a maximum of 72 h. In our hands, the fluorescence of the transfected RNP complex started to decline after 48 h and almost no or very little fluorescence was visible after 72 h. We screened for RNP-containing fluorescent cells at 48 h after the laser pulse (Figure 2A, A'), identified and selected RNP-containing cells and excised small leaf tissue fragments of different sizes (0.1–0.3 cm radius) depending on the intensity and distribution of the RNP fluorescence signal (Figure 2A"). The selected leaf fragments looked healthy at 48 h and were grown on MS medium to regenerate intact plantlets (Figure S3).

3.3-Rapid and reliable identification of *pds* mutant tobacco plants

Loss-of-function mutations in the *PDS* gene generate an albino phenotype, which allows the efficiency of genome editing to be determined by the visual inspection of regenerated plantlets (Hidalgo-Grass & Strahilevitz, 2010; Denbow et al., 2018). Following regeneration, we used a simple PCR-based HRMA procedure to identify the mutants. We analyzed 1673 plants from the *pds* experiment and identified 147 homozygous/biallelic mutants and 442 heterozygous mutants. Representative images of homozygous *pds* mutant plants with the anticipated albino phenotypes (homozygous lines F19, I26, L35 and T10) are provided in Figures 2B and S4. The distinct melting curves of *pds* homozygous mutant T10 and the wild-type control are compared as an example in Figure 2C. The homozygous/biallelic mutants were characterized in more detail by Sanger sequencing across the target site, revealing 93 homozygous and 54 biallelic mutants, confirming the positive HRMA results (Figure 2D, E). The plant generation and the

line name, as well as the respective particular mutation and zygosity, are given in the Table S5. A representative chromatogram is provided for line T10, showing a deletion upstream of the protospacer adjacent motif (PAM; Figure S5). Our new pulsed laser-induced shockwave method achieved an overall mutation efficiency of 35.2% for the *PDS* gene (Figures 2D and S6).

3.4-Generation of *adf* mutant tobacco plants and characterization under osmotic stress

We used the same HRMA method discussed above to screen 1011 plants from the *adf* experiment and identified 57 homozygous/biallelic mutants and 110 heterozygous mutants. In the former group, Sanger sequencing confirmed the positive HRMA results and resolved 48 homozygous mutants (e.g., lines A3, A57, A61, B2 and C60) and 9 biallelic mutants (e.g., lines C66 and C72). The distinct melting curves of *adf* homozygous mutant A57 and the wild-type control are compared as an example in Figure 3A, along with the chromatogram of line A57 showing a single-base deletion (Figure S7). The percentage of plants bearing a mutation, either homozygous, biallelic or heterozygous was 16.5% (Figure 3B). The plant generation, the line designation as well as the respective particular mutation and zygosity are shown in Table S6. Here we observed predominantly a single base pair deletion. Representative mutation patterns observed for the homozygous, biallelic and heterozygous mutants are shown in Figure 3C.

To visualize the actin filaments under normal irrigation conditions, we stained three homozygous mutant T_0 *adf* plants (A57, A67 and B2) and wild-type controls with phalloidin. Confocal microscopy confirmed the presence of more actin filaments in the leaves of the mutant plants (Figure S8B) than wild-type controls (Figure S8A). Furthermore, a standard test of cell membrane thermostability in 10 randomly selected (homozygous or biallelic) *adf* T_0 mutants and wild-type controls under normal irrigation conditions revealed significantly higher membrane stability among the mutants (Figure 3I).

3.5-Heritability of the *adf* mutation in generations T_1 and T_2

After confirmation of mutations at the T_0 stage using HRMA and Sanger sequencing, *adf* mutant plants (all the homozygous and biallelic events in Table S6) were allowed to grow and set seed under controlled conditions in the greenhouse. After selfing, 30% of T_0 events did not set seeds, 33% of events set very few seeds, 10% of events set a few seeds but at a later time than wild-type plants (approximately 1-2 months delay). 27% of events set seeds in a manner almost similar to wild-type plants in terms of quality of seeds and time for seed setting. We grew T_1 plants from 13 different T_0 events and confirmed the presence of the mutation by HRMA and Sanger sequencing (Figure S9A, A'). These plants set fewer seeds compared to wild-type plants, but the quality of the seeds and the time for seed setting were similar to wild-type plants. The mutations were stably transmitted to the next generations. Among the 13 mutants, all of them had the same homozygous mutation except C31 and C72, which both harboured a biallelic mutation (Table S6). We then generated T_2 plants by selfing 10 T_1 events (8 homozygous mutants and 2 biallelic mutants) for subsequent analysis under abiotic stress, and again confirmed the presence of the expected mutations by HRMA and Sanger sequencing (Figure S9B and B').

3.6-Actin enrichment and membrane stability in *adf* homozygous mutant plants

T_2 homozygous *adf* mutant plants (lines A57, A67 and B2) were stained with phalloidin to visualise actin enrichment and the formation of interlocking marginal lobes (IMLs). Figure 3D is a schematic representation of the apical cell membrane and cell–cell junction, which we used to determine the ratio of actin accumulation**.** Figure 3E, F shows the Z projections of the apical cell membrane. The graph in Figure 3G shows the ratio of actin intensity in the apical cell membrane and cell–cell junction. Higher levels of actin were detected in the cell membrane of the mutant lines, along with the formation of IMLs (Figure 3E, E', F and F'). In the *adf* mutants, actin filaments were clustered at the cell–cell junctions, but this was not observed in wild-type controls (Figure 3E, E', F and F'). This resulted in a high ratio of actin accumulation favouring the cell–cell junctions in the *adf* mutant lines (Figure 3G) and an increase in the number of IMLs in the mutant cells (Figure 3H). These data, together with our previous results (Augustine et al., 2015), suggest that the accumulation of actin facilitates the formation of IMLs in the *adf* mutant plants (Figure S8C). A potential mechanism underlying the accumulation of cortical actin and IML formation in *adf* mutants is proposed in Figure S8D.

The drought tolerance of the *adf* mutant plants (10 independent mutants) was assessed by inducing soil moisture stress at the 4–6-leaf stage and measuring membrane injury using a conductivity meter, which is a widely accepted measure of drought tolerance based on membrane stability. Drought stress was applied for 5 days before the reintroduction of normal irrigation. We tested cell membrane stability (CMS) on day 0 before the stress treatment, on day 5 of stress, and 5 days after the reinstatement of normal irrigation conditions (Figure 4A). Representative images of mutant and wild-type tobacco plants at the same time points are shown in Figure 4B. More mutant lines under drought stress are given in Figure S10. The *adf* mutant plants (A57, A67, A672, A69, A90, B2, C6, C31, C60 and C72) showed significantly higher membrane stability under both normal irrigation and drought stress conditions. As the soil moisture level declined, the degree of cell membrane injury fell by 1–7% in the *adf* mutant plants but did not change in the wild-type controls, indicating that the mutant plants can adapt to soil moisture stress. The 10 mutant lines showed an injury rating ranging from 80% (line C60) to 86% (line C31) compared to 98% in the wild-type plants (Figure 4C). One possible explanation for this difference in injury rating might be that all mutant plants harbour the same mutation, except C31 and C72. These two mutants were chosen for drought stress analysis because they showed good seed quality at the T_0 stage. Under drought stress, C31 and C72 showed higher cell membrane injury (86% and 85%, respectively) compared to all other analysed mutants. C31 was showing 86% of membrane injury, which resulted in low tolerance to drought stress similar to wild-type plants (Figure S11**)**.

3.7-Leaf water content under drought stress in the *adf* mutant plants

The RWC of the 10 T_2 *adf* mutant plant lines was higher than that of wild-type plants under drought stress. On day 0 before soil moisture stress was applied, the RWC of the mutant and wild-type plants was similar at ~50%. After 5 days of drought, the RWC of wild-type plants had dropped to ~15%, whereas it remained significantly higher in the mutant plants, ranging between ~40% in lines A57, A67 and C60 to

~30% in line C6. Furthermore, the RWC of the mutant plants recovered (~50%) after 5 days of normal irrigation, whereas the wild-type plants still showed a low RWC of ~10% (Figure 4E). We also obtained a slow wilting phenotype with high RWC in all the mutants compared to wild-type plants. A previous report on wheat mutant RYNO3926 also displayed a full recovery in RWC after re-watering (le Roux et al., 2020). The authors suggested that the mutant can likely readjust its osmoregulation assuming full turgor pressure and can activate its metabolic activity, providing whole-plant relief to the water stress (Souza et al., 2004; le Roux et al., 2020).

3.8-Stress-responsive genes are induced in the *adf* mutant plants

For a comparative analysis of stress-responsive gene expression, we selected the four homozygous mutant lines showing the highest cell membrane stability (A57, A67, A69 and C60) as well as one with lower membrane stability and biallelic mutation (C31). The phenotype of C31 after 5 days of drought stress is shown in Figure S11. We quantified the transcripts of *adf* and four stress-responsive genes encoding the proteins Hsp70, WRKY, ERF and DREB2 after 5 days of drought stress using the comparative CT method. In the four mutants with stable membranes and homozygous mutation, *adf* was induced minimally (0.93–1.5-fold), whereas the same gene was induced 4.5-fold in line C31 and 55.7-fold in wild-type plants under drought stress compared to normally irrigated wild-type plants (Figure 4D). We measured the expression of the four drought-inducible genes in the mutant plants relative to the wild-type controls. In the four mutants with the highest membrane stability, these genes were strongly induced by drought (50.2–132.3-fold for Hsp70, 58.7–108.3-fold for ERF, 54.19–138.85-fold for DREB2, and 55.33–77.17-fold for WRKY), with C60 showing the strongest responses and the most stable membranes (Figure 4F–I). The same four genes were only moderately induced in line C31 (8.63-fold for Hsp70, 10.33-fold for ERF, 18.25-fold for DREB2 and 15.88-fold for WRKY).

3.9-T_2 generation *adf* mutants tolerate high salinity

Finally, we carried out seed germination tests in soil using different salt concentrations (100, 200 and 300 mM NaCl). The 13 mutants and the wild-type plants were morphologically similar when grown without NaCl (Figure 5A). The wild-type plants were unable to germinate in all three treated soils, indicating susceptibility to excess salinity (Figure 5B-D). In contrast, the mutant plants germinated and survived for the entire testing period (4 weeks) under all three salinity conditions, although there was an inverse relationship between shoot height and salt concentration. We measured the relative expression levels of the four stress-responsive genes at 300 mM NaCl in six mutants varying in germination efficiency and percentage (A67, C6, C60, A90, C31 and A69). We found that all four genes were upregulated in the mutant lines (4.43–19.6-fold for DREB2, 4.84–17.85-fold for WRKY, 3.65–7.51-fold for Hsp70 and 1.97–19.65-fold for ERF) compared to wild-type plants (Figure 5E–H). Lines C60, A90 and A69 showed the highest induction of stress-responsive gene expression, corresponding to their better germination and survival rates under salinity stress.

Discussion

CRISPR/Cas9 is the most versatile and widely-used genome-editing tool, facilitating the targeted mutagenesis of various loci in many different plant species (Li et al., 2015). We have described a new method for genome editing in plants that combines cavitation bubble-induced shockwaves for the transfection of plant cells with fluorescent RNPs, fluorescence microscopy to confirm transfection, regeneration based on visual selection, and HRMA to screen the mutant plants. The combination of these techniques allowed the rapid selection of tissues for regeneration following DNA-free genome editing. Our experiments demonstrated for the first time the successful delivery of RNPs into intact plant cells using cavitation bubble-induced shock waves generated by a pulsed laser. In our study, the cavitation bubbles were formed after optical breakdown induced by a femtosecond pulsing laser. These lasers are quite expensive and are not accessible to many laboratories, but it is possible to get access to such infrastructure. However, previous studies in mammalian corneal cells showed the possibility to achieve the same optical breakdown using nanosecond and picosecond pulsed lasers (Juhasz et al., 1994; Cherian and Rau 2008). Presumably, these lasers can also be used to shuttle RNPs into plant cells; they are more affordable and lower the investment costs for using our approach.

The efficient delivery of RNPs is a central requirement to achieve DNA-free genome editing. Particle bombardment, electroporation, PEG-mediated transfection and microinjection all suffer from low efficiency of RNP delivery into intact plant cells (Eeckhaut et al., 2013; Altpeter et al., 2016; Svitashev et al., 2016; Zhang et al., 2020). For example, the biolistic transformation efficiency in different species varies between 4%-20% (Cruz et al., 2009; Gatica-Arias et al., 2013; Yadav et al., 2013; Nicolia et al., 2015). Compared to biolistics, our transformation method generated more mutant regenerants (35.2% in *PDS* and 16.5% in *ADF*). Our newly developed genome editing toolbox is fast, easy to perform, reproducible and shows several advantages compared to existing techniques: (1) the high spatial controllability of laser energy makes it suitable for the treatment of intact leaf material; (2) unlike PEG-mediated transfection, our method allows the direct introduction of RNPs into intact plant cells rather than protoplasts, thus (3) reducing the time required for regeneration of plantlets and (4) the method might be applicable to species that cannot yet regenerate from protoplasts. Presumably, the cavitation bubble-induced shockwaves for protein delivery into intact plant tissue are gentle and reduces cell damage, i.e. preserves a larger population of intact transfected cells. The combination with fluorescent-labelled RNPs facilitates the isolation of the transfected cells and tissue segments, thus increasing the likelihood of obtaining a higher rate of regeneration efficiency of the mutated plants. Further advantages include the omission of pathogens (such as *Agrobacterium*) infection and of specialized vectors for the transfer of DNA or protein or RNA. A timeline for the new DNA-free genome editing method is provided in Figure S6.

RNP-mediated genome editing has been laborious thus far because the absence of a selectable marker requires a time-consuming screening process to identify rare mutants in a large background of wild-type cells. In our experiments, the ATTO-550-labeled tracrRNA allowed the rapid identification of transfected cells by fluorescence microscopy. In general, fluorescence-activated cell sorting (FACS) is also possible to select transfected protoplasts, but keeping the protoplasts alive after sorting is challenging due to their fragile nature (Bardmann and Birnhaum 2010). By selecting the region containing cells transfected with RNPs, we were able to avoid large numbers of wild-type cells, thereby facilitating the selective

regeneration of mutants. We used commercially purchased HiFi Cas9 protein and ATTO-550-labeled tracrRNA, which are affordable and their use guarantees quick nuclease activity (Vakulskas et al., 2018) and easy visual identification of RNP containing cells. Regenerated plants were subjected to a PCR-based HRMA procedure and mutants were easily identified because this method can resolve sequences with single-nucleotide changes (Hidalgo-Grass & Strahilevitz 2010; Denbow et al. 2018; Li et al. 2018). HRMA has been described as simpler, more sensitive, more specific, less expensive and quicker than other mutation identification methods (McKinney et al. 2004; Willmore et al. 2004; Zhou et al. 2004; Kennerson et al. 2007; Hung et al. 2008; Samarut et al. 2016). Using HRMA, we were able to screen 96 plants in 2 h, a much higher throughput than we previously achieved using the T7 assay for the detection and selection of mutants (Bortesi et al. 2017). The main limitation of HRMA is that the exact mutation pattern cannot be identified, so it must be used in conjunction with Sanger sequencing. However, because HRMA is inexpensive and efficient, we believe that it is now one of the preferred genome editing screening methods. Thus, gDNA regions of HRMA positively tested plants were PCR-amplified and subjected to Sanger sequencing to determine the exact nature of the mutations. The combination of the new transfection technique combined with the improved selection process resulted in the regeneration of numerous gene-edited plants at high mutation efficiencies of 16.5% for the *ADF* and 35.2% for the *PDS* gene.

The biological effect of the *PDS* gene mutation was easily verified by visual screening. *ADF* proteins are key modulators of the actin cytoskeleton, and the downregulation of *ADF* promotes actin polymerization, which can be visualized using phalloidin (Chun-Hai et al. 2001; Augustine et al. 2015; Chang et al. 2015). The principal components of the actin cytoskeleton include monomeric actin (G-actin) and filamentous actin (F-actin), with G-actin being the dominant form (Nan et al. 2017; Wioland et al. 2017). *ADF* depolymerizes F-actin to G-actin. Loss-of-function mutations in the *ADF* gene should therefore promote the formation of more F-actin. To analyze how the mutation in the *ADF* gene affected cellular and molecular processes, we stained T_0 *adf* mutant plants with fluorescent phalloidin to visualize the anticipated enhanced formation of actin filaments. The relationship between *ADF*s and abiotic stress tolerance is still unknown. In a previous study, we showed that the downregulation of *ADF* in transgenic sugarcane plants overexpressing Hsp70 increased cell membrane stability, actin accumulation, and the formation of IMLs, thus contributing to osmotic stress tolerance (Augustine et al. 2015). Here, the quantitative real-time experiments show that the *adf* mutant lines have a significant under expression of *ADF* mRNA level (Figure 4D). The *ADF* gene was induced 2500-fold in sugarcane under drought stress compared to irrigated control plants, which showed lower membrane stability, no actin accumulation and IML formation, resulting in a more sensitive phenotype to drought stress (Augustine et al. 2015). We have also previously shown that IMLs in the abovementioned transgenic sugarcane plants and in native sweetcane (*Erianthus arundinaceus*) plants disappear when actin polymerization is inhibited using latrunculin A. This confirmed the role of filamentous actin in the maintenance and formation of IMLs and, therefore, in stress tolerance (Augustine et al., 2015). The transgenic sugarcane plants were able to survive 10 days in soil with only 8.1% moisture and were able to germinate in 300 mM NaCl (Augustine et al. 2015). Consistent with the above study, we observed significantly higher membrane stability followed

by actin accumulation and the formation of IMLs under normal and drought stress conditions in *adf* mutant tobacco plants, resulting in higher drought and salinity stress tolerance.

Interestingly, our results showed a reduction in the transcript level of the CRISPR-targeted *ADF* gene. A previous report on Methicillin-resistant *Staphylococcus aureus* (MRSA) described a similar effect on the transcription of the *mecA* methicillin resistance gene in CRISPR-treated samples, which was reduced by 77% (Wang et al, 2017). Other studies (Tuladhar et al, 2019; Janik et al., 2020) also reported changes in the transcript or protein expression in CRISPR-targeted genes in mammalian cell lines and concluded that this was likely due to on-target mRNA misregulation. According to the authors, mRNA splicing is a complex phenomenon and more research is needed to evaluate the potential effects of indels on mRNA regulation (Tuladhar et al., 2019).

Taken together, our results show that cavitation bubble-induced shockwaves generated by a pulsed laser can achieve the efficient transfection of walled plant cells with RNPs, even in the context of intact tissue explants. When used to deliver preassembled CRISPR/Cas9 components, targeted mutations were achieved with high efficiency. This method greatly simplifies the production of genome-edited plants, avoids the need to regenerate plants from protoplasts, and is potentially transferable to any plant species that can be regenerated in tissue culture, providing an opportunity to extend genome editing to currently recalcitrant plant species. In the longer term, this technique may accelerate the development of novel crops that address the needs of a growing population and the effects of climate change. We showed that the accumulation of actin filaments on the plant cell membrane plays a major role in stress tolerance by stabilizing the membrane, indicating a key role in osmotic stress tolerance. This *ADF* genome editing study demonstrates that single endogenous genes can be modified to create novel variants that have a significantly positive effect on a complex trait such as drought and salinity stress tolerance. New crop varieties that produce more actin filaments could therefore be used to expand agricultural production to marginal soils.

Declarations

Author Contributions

SA conceptualized, performed and analyzed the work. AVC and KS performed the experiments. AVC and SDF provided technical and helpful discussions. SA, SDF, NR, UC and SS wrote and edited the manuscript. All the authors read and approved the manuscript.

Acknowledgment

This research work was supported by the Federal Ministry of Education and Research (BMBF), Germany, grant number FKZ 031B0536. We thank Dr Richard M. Twyman for editorial assistance.

Data availability statement

The data that support the findings of this study are available from the corresponding author upon reasonable request.

References

Altpeter, F., Springer, N.M., Bartley, L.E., Blechl, A.E., Brutnell, T.P., Citovsky, V., Conrad, L.J., Gelvin, S.B., Jackson, D.P., Kausch, A.P., et al. (2016). Advancing Crop Transformation in the Era of Genome Editing. *The Plant Cell* 28:1510–1520.

Augustine, S.M., Cherian, A.V., Syamaladevei, D.P. & Subramonian, N. (2015). Erianthus arundinaceus HSP70 (EaHSP70) acts as a key regulator in the formation of anisotropic interdigitation in sugarcane (Saccharum spp. hybrid) in response to drought stress. *Plant and Cell Physiology* 56:2368-2380.

Bargmann, B.O.R. & Birnbaum, K.D. (2010). Fluorescence Activated Cell Sorting of Plant Protoplasts. *Journal of Visualized Experiments* 36: 1673.

Barrs, H.D., & Weatherley, P.E. (1962). A re-examination of the relative turgidity technique for estimating water deficits in leaves. *Australian Journal of Biological Sciences* 15:413–428.

Bortesi, L., Augustine, S.M., Fischer, R., Sack, M., & Zischewski, J. EU3392339. (2017). Improved genome editing in plant cells. (Patent application no. 17166753.8.).

Chang, C.Y., Jyh-Der, L., & Yi-Jang, L. (2015). The Actin Depolymerizing Factor (ADF)/Cofilin Signaling Pathway and DNA Damage Responses in Cancer. *International Journal of Molecular Sciences*. 16:4095–4120.

Cherian, A.V & Rau, K.R. (2008). Pulsed-laser-induced damage in rat corneas: time-resolved imaging of physical effects and acute biological response. *Journal of Biomedical Optics*. 13(2):024009.

Chomczynski, P., & Mackey, K. (1995). Modification of the TRI reagent DNA/protein isolation procedure for isolation of RNA from polysaccharide and proteoglycan rich sources. *BioTechniques* 19:942–945.

Chun-Hai D, Xia GX, Hong Y, Ramachandran S, Kost B, & Chua NH. (2001). ADF proteins are involved in the control of flowering and regulate F-Actin organization, cell expansion, and organ growth in Arabidopsis. *The Plant Cell* 13:1333–1346.

Collins, T.J. (2007). ImageJ for microscopy. *BioTechniques* 43: S25–S30.

Cruz, A.R.R., Soares, E.L., Campos, F.A.P., & Aragão, F.J.L. (2009) Biolistic-mediated genetic transformation of prickly-pear cactus (Opuntia ficus-indica Mill.). *Acta Horticulturae* 811:255–257.

Denbow, C., Ehivet, S. C. & Okumoto, S. (2018). High Resolution Melting Temperature Analysis to Identify CRISPR/Cas9 Mutants from Arabidopsis. *Bio Protocol* 8: e2944.

Gatica-Arias, A., Weber, G. (2013). Genetic transformation of hop (Humulus lupulus L. cv. Tettnanger) by particle bombardment and plant regeneration using a temporary immersion system. *In Vitro Cellular & Developmental Biology* 49:656–664.

Guha, T.K., Wai, A., & Hausner, G. (2017). Programmable genome editing tools and their regulation for efficient genome engineering. *Computational and Structural Biotechnology Journal* 15:146–160.

Hidalgo-Grass C & Strahilevitz J. (2010). High-Resolution Melt Curve Analysis for Identification of Single Nucleotide Mutations in the Quinolone Resistance Gene aac(6')-Ib-cr. *Antimicrobial Agents and Chemotherapy* 54:3509–3511.

Hung, C., Lee, C., Chang, C., Jong, Y., Chen, C., Hseih, W., Su, Y. & Lin, W. (2008). Genotyping of the G1138A mutation of the FGFR3 gene in patients with achondroplasia using high-resolution melting analysis. *Clinical Biochemistry* 41:162–166.

Janik, E., Niemcewicz, M., Ceremuga, M., Krzowski, L., Saluk-Bijak, J., & Bijak, M. (2020). Various Aspects of a Gene Editing System—CRISPR–Cas9. *International Journal of Molecular Sciences* 21:9604.

Jeffry, D.S., & Joung, J.K. (2014). CRISPR-Cas systems for genome editing, regulation and targeting. *Nature Biotechnology* 32 (4): 347–355.

Juhasz, T., Hu, X.H., Laszlo, T., & Bor, Z. (1994). Dynamics of shock waves and cavitation bubbles generated by picosecond laser pulses in corneal tissue and water. *Lasers in Surgery and Medicine* 15(1):91–98.

Kawall, K. (2019). New Possibilities on the Horizon: Genome Editing Makes the Whole Genome Accessible for Changes. *Frontiers in Plant Science* 10:525.

Kennerson, M., Warburton, T., Nelis, E., Brewer, M., Polly, P., De Jonghe, P., Timmerman, V. & Nicholson, G. (2007). Mutation scanning the GJB1 gene with high-resolution melting analysis: implications for mutation scanning of genes for Charcot–Marie–Tooth disease. *Clinical Chemistry* 53:349–352.

Kobayashi, Y., Kobayashi, I., Funaki, Y., Fujimoto, S., Takemoto, T. & Kunoh, H. (1997). Dynamic reorganization of microfilaments and microtubules is necessary for the expression of non-host resistance in barley coleoptile cells. *The Plant Journal* 11:525–537.

le Roux, M.L., Burger, N., Vlok, M., Kunert, K.J., Cullis, C.A., & Botha, A.M. (2020). Wheat Line "RYNO3936" Is Associated With Delayed Water Stress-Induced Leaf Senescence and Rapid Water-Deficit Stress Recovery. *Frontiers in plant science* 11:1053.

Leighton T.G. (1995). Bubble population phenomena in acoustic cavitation. *Ultrasonics Sonochemistry* 2: (2).

Li, J.F., Zhang, D., & Sheen J. (2015). Targeted plant genome editing via the CRISPR/Cas9 technology. *Methods in Molecular Biology* 1284:239-55.

Li, S., Liu, S., Liu, Y., Lu, H., Tan, Y., Huang, J., Wei, P., & Shu, Q.Y. (2018). HRM-facilitated rapid identification and genotyping of mutations induced by CRISPR/Cas9 mutagenesis in rice. *Crop Breeding and Applied Biotechnology* 18:184–191.

Lin, C.S., Hsu, C.T., Yang, L.H., Lee, L.Y., Fu, J.Y., Cheng, Q.W., Wu, F.H., Hsiao, H.C.W., Zhang, Y., Zhang, R., Chang, W.J., Yu, C.T., Wang, W., Liao, L.J., Gelvin, S.B., & Shih, M.C. (2018). Application of protoplast technology to CRISPR/Cas9 mutagenesis: from single-cell mutation detection to mutant plant regeneration. *Plant Biotechnology Journal* 16:1295–1310.

Liu, Y., Yang, H., & Sakanishi, A. (2006). Ultrasound: Mechanical gene transfer into plant cells by sonoporation. *Biotechnology Advances* 24:1–16.

Livak, K.J., & Schmittgen, T.D. (2001). Analysis of relative gene expression data using real time quantitative PCR and the 2−CT method. *Methods* 25:402–408.

Mao, Y., Botella, J.R., Liu, Y., & Zhu, J.K. (2019). Gene editing in plants: progress and challenges. *National Science Review* 6: 421–437.

Maochen, W., Yi, Z., Chenliang, C., Juan, T., Xiasheng, G., & Dong, Z. (2018). Sonoporation-induced cell membrane permeabilization and cytoskeleton disassembly at varied acoustic and microbubble-cell parameters. *Scientific Reports* 8:3885

Martineau, J.R., Specht, J.E., Williams, J.H., & Sullivan, C.Y. (1979). Temperature tolerance in soybeans. I. Evaluation of a technique for assessing cellular membrane thermostability. *Crop Science* 19:75–78.

McKinney, J., Longo, N., Hahn, S., Matern, D., Rinaldo, P., Strauss, A. & Dobrowolski, S. (2004). Rapid comprehensive screening of the human medium chain acyl-CoA dehydrogenase gene. *Molecular Genetics and Metabolism* 82:112–120.

Mickael, M., Roberto, V., Min-Hee, J., Ok-Jae, K., Seokjoong, K., Jin-Soo, K., et al. (2016). DNA-free genetically edited grapevine and apple protoplast using CRISPR/Cas9 ribonucleoproteins. *Frontiers in Plant Science* 7:1904.

Miller, D.L., Pislaru, S.V., & Greenleaf, J.F. (2002). Sonoporation: mechanical DNA delivery by ultrasonic cavitation. *Somatic Cell and Molecular Genetics* 27:115–134.

Molaei, P., Namvar, A.E.A., & Bejandi, T.K. (2012). Water relation, solute accumulation and cell membrane injury in sesame (Sesamum indicum L.) cultivars subjected to water stress. *Annals of Biological Research* 3:1833–1838.

Nan Q, Qian D, Niu Y, He Y, Tong s, Niu Z, Ma J, Yang Y, An L, Wan D & Xiang Y. (2017). Plant Actin-Depolymerizing Factors possess opposing biochemical properties arising from key amino acid changes throughout evolution. *The Plant Cell* 29:395–408.

Nicolia, A., Proux-Wéra, E., Åhman, I., Onkokesung, N., Andersson, M., Andreasson, E., & Zhu, L.-H. (2015). Targeted gene mutation in tetraploid potato through transient TALEN expression in protoplasts. *Journal of Biotechnology* 204: 17–24.

O'Brien, J.A., & Lummis, S.C.R. (2011). Nano-biolistics: a method of biolistic transfection of cells and tissues using a gene gun with novel nanometer-sized projectiles. *BMC Biotechnology* 11:66.

O'Brien, J.A., Holt, M., Whiteside, G., Lummis, S.C.R., & Hastings, M. (2001). Modifications to the hand-held Gene Gun: improvements for in vitro Biolistic transfection of organotypic neuronal tissue. *Journal of Neuroscience Methods* 112:57–64.

Opalski, K.S., Schultheiss, H., Kogel, K.H. & Huckelhoven, R. (2005). The receptor like MLO protein and the RAC/ROP family G-protein RACB modulate actin reorganization in barley attacked by the biotrophic powdery mildew fungus Blumeria graminis f. sp hordei. *The Plant Journal* 41:291–303.

Ortigosa, A., Gimenez-Ibanez, S., Leonhardt, N., & Solano, R. (2018). Design of a bacterial speck resistant tomato by CRISPR/Cas9-mediated editing of SlJAZ2. *Plant Biotechnology Journal* doi:https://doi.org/10.1111/pbi.13006.

Pospíšilová, J., Wilhelmová, N., Synková, H., Čatský, J., Krebs, D., Tichá, I., Hanáčková, B., & Snopek, J. (1998). Acclimation of tobacco plantlets to ex vitro conditions as affected by application of abscisic acid. *Journal of experimental Botany* 49:863-869.

Sack, M., Rademacher, T., Spiegel, H., Boes, A., Hellwig, S., Drossard, J., Stoger, E. & Fischer, R. (2015). From gene to harvest: insights into upstream process development for the GMP production of a monoclonal antibody in transgenic tobacco plants. *Plant Biotechnology Journal* 13:1094-105.

Samarut, E., Lissouba, A. and drapeau, P. (2016). A simplified method for identifying early CRISPR-induced indels in zebrafish embryos using high resolution melting analysis. *BMC Genomics* 17: 547.

Sant'Ana, R.R.A., Caprestano, C.A., Nodari, R.O., Agapito-Tenfen, S.Z. (2020). PEG-Delivered CRISPR-Cas9 Ribonucleoproteins System for Gene-Editing Screening of Maize Protoplasts. *Genes* 11:1029.

Schiml, S., & Puchta, H. (2016). Revolutionizing plant biology: multiple ways of genome engineering by CRISPR/Cas. *Plant Methods* 12:8.

Sedeek, K.E.M., Mahas, A., & Mahfouz, M. (2019). Plant genome engineering for targeted improvement of crop traits. *Frontiers in Plant Science* 10:114.

Souza, R., Machado, E., Silva J., Lagôa, A., & Silveira, J. (2004). Photosynthetic gas exchange, chlorophyll fluorescence and some associated metabolic changes in cowpea (Vigna unguiculata) during water stress and recovery. *Environmental and Experimental Botany* 51: 45–56.

Tachibana, K., Uchida, T., Ogawa, K., Yamashita, N., & Tamura K. (1999). Induction of cell-membrane porosity by ultrasound. *The Lancet* 353:1409.

Thomas, J.L., Bardou, J., Hoste, S.L., Mauchamp, B., & Chavancy, G. (2001). A helium burst biolistic device adapted to penetrate fragile insect tissues. *Journal of Insect Science* 1:9.

Tuladhar, R., Yeu, Y., Tyler Piazza, J. et al. (2019). CRISPR-Cas9-based mutagenesis frequently provokes on-target mRNA misregulation. *Nature Communication*s 10: 4056.

Vakulskas, C., Dever, D., et al. (2018) A novel high-fidelity Cas9 delivered as a ribonucleoprotein complex enables high frequency gene editing in human haematopoietic stem and progenitor cells. *Nature Medicine* 24:1216-1224.

Wang, F., Wang, C., Liu, P., Lei, C., Hao, W., Gao, Y., et al. (2016). Enhanced rice blast resistance by CRISPR/Cas9-targeted mutagenesis of the ERF transcription factor gene OsERF922. *PLoS One* 11:e0154027.

Wang, H., Russa, M.L., & Qi, L.S. (2016). CRISPR/Cas9 in genome editing and beyond. *Annual Review of Biochemistry* 85:227–64.

Wang, K., & Nicholaou, M. (2017). Suppression of Antimicrobial Resistance in MRSA Using CRISPR-dCas9. Am. Soc. *Clinical Laboratory Science* 30: 207.

Willmore, C., Holden, J., Zhou, L., Tripp, S., Wittwer, C. & Layfield, L. (2004). Detection of c-kit-activating mutations in gastrointestinal stromal tumors by high-resolution amplicon melting analysis. *American Journal of Clinical Pathology* 122:206–216.

Wioland H, Guichard B, Senju Y, Myram S, Lappalainen P, Jegou A & Romet-Lemonne G. (2017). ADF/Cofilin accelerates actin dynamics by severing filaments and promoting their depolymerization at both ends. *Current Biology* 27:1956–1967

Woo, J.W., Kim, J., Kwon, S.I., Corvalan, C., Cho, S.W., Kim, H., et al. (2015). DNA-free genome editing in plants with preassembled CRISPR-Cas9 ribonucleoproteins. *Nature Biotechnology* 33:1162–4.

Yadav, T., Kachhwaha, S. & Kothari, S.L. (2013). Efficient in vitro plant regeneration and generation of transgenic plants in barley (Hordeum vulgare L.) using particle bombardment. *Journal of Plant Biochemistry and Biotechnology* 22: 202–213.

Yao, L., Zhang, Y., Liu, C., Liu, Y., Wang, Y., Liang, D., et al. (2018). OsMATL mutation induces haploid seed formation in indica rice. *Nature Plants* 4:530–3.

Yi, Z., Zhen, L., Yuan, Z., Yanpeng, W., Jinxing, L., Kunling, C., Jin-Long, Q., & Caixia, G. (2016). Efficient and transgene-free genome editing in wheat through transient expression of CRISPR/Cas9 DNA or RNA. *Nature Communication 7*:12617.

Zhang, Y., Bai, Y., Wu, G., Zou, S., Chen, Y., Gao, C., & Tang, D. (2017). Simultaneous modification of three homoeologs of TaEDR1 by genome editing enhances powdery mildew resistance in wheat. *The Plant Journal* 91:714.

Zhang, Y., Iaffaldano, B. & Qi, Y. (2021). CRISPR ribonucleoprotein-mediated genetic engineering in plants. *Plant communications* 2:100168.

Zhang, Y., Pribil, M., Palmgren, M. and Gao C (2020). A CRISPR way for accelerating improvement of food crops. *Nature Food* 1:200-205.

Zhou, J., Peng, Z., Long, J., Sosso, D., Liu, B., Eom, J.S., et al. (2015). Gene targeting by the TAL effector PthXo2 reveals cryptic resistance gene for bacterial blight of rice. *The Plant Journal* 82:632–43.

Zhou, L., Vandersteen, J., Wang, L., Fuller, T., Taylor, M., Palais, B. & Wittwer, C. (2004). High-resolution DNA melting curve analysis to establish HLA genotypic identity. *Tissue Antigens* 64:156–164.

Figures

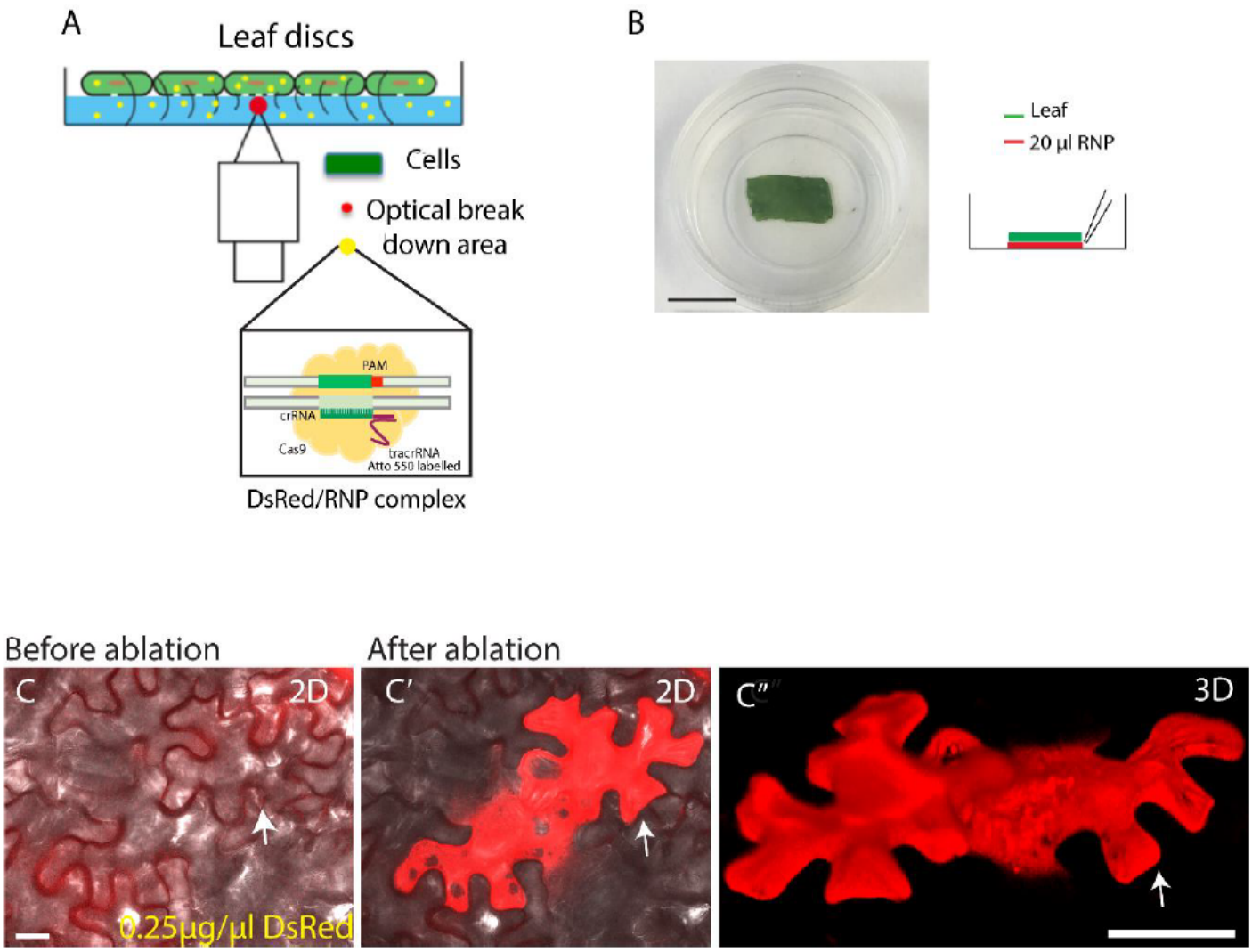

Figure 1

Cavitation bubble-induced shockwaves promote the transfer of DsRed/RNPs into intact tobacco cells. (A) Schematic representation of the laser setup. (B) Representative tobacco leaf sample used for DsRed/RNP transfection on a microscopic-grade Petri dish. Scale bar = 1 cm. (C) Confocal microscope image of tobacco leaf sections before laser-assisted transfection. The white arrow points to the region chosen for laser treatment. Scale bar = 50 µm. (C'). The same region 10 min after the shockwave-mediated uptake of 20 µL DsRed solution (0.25 µg µL-1). DsRed fluorescence was detected by confocal microscopy. (C") 3D reconstruction of DsRed-positive cells 10 min after laser treatment. The white arrow points to the region chosen for laser treatment. Scale bar = 50 µm.

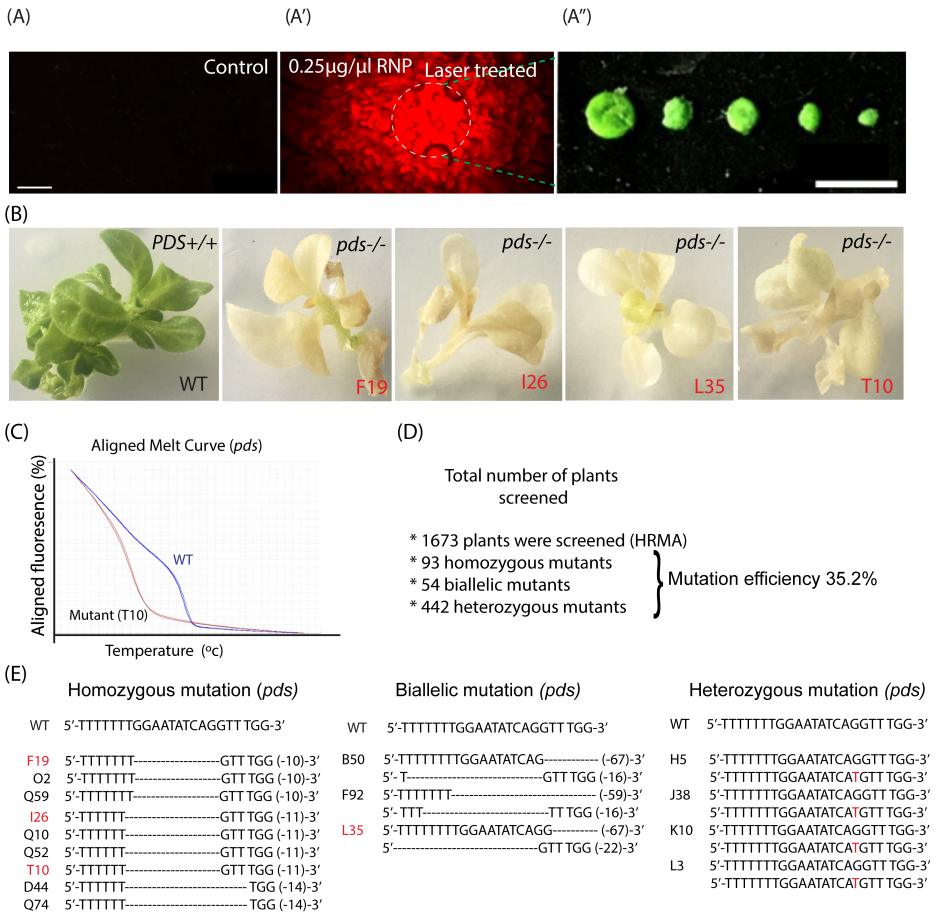

Figure 2

Analysis of RNP-mediated PDS mutations in T0 plants. (A) Non-transfected tobacco leaf section does not show any fluorescence. Scale bar = 50 µm. (A') Detection of ATTO-550-labeled fluorescent RNPs by fluorescence microscopy in cells 10 min after laser-assisted transfection. Scale bar = 50 µm. (A") Representative sampling of RNP-containing regions of different sizes (0.1–0.3 cm in radius) depending on the intensity of the RNP signal. Scale bar = 1 cm. (B) Albino pds homozygous mutant lines F19, I26,

L35 and T10 compared to a wild-type (WT) plant. (C) Representative image showing the high-resolution melt analysis of a pds mutant (line T10, red line) compared to wild-type (WT) (blue line). (D) Representation of the pds gene mutation efficiency. (E) Alignments of representative genome-edited mutants. The mutants marked in red correspond to the albino mutant lines in (B).

(A)

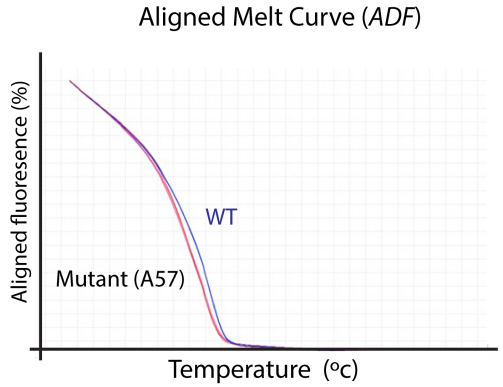

(B)

Total number of plants screened

* 1011 plants were screened (HRMA)
* 48 homozygous mutants
* 9 biallelic mutants
* 110 heterozygous mutants

} Mutation efficiency 16.5%

(C)

Homozygous mutation (*adf*)

WT	5′-CTTGGAGCTGAAGAGGAAGA AGG-3′
A3	5′-CTTGGAGCTGAAGAGGA--GA AGG (-1)-3′
A57	5′-CTTGGAGCTGAAGAGGA--GA AGG (-1)-3′
A61	5′-CTTGGAGCTGAAGAGGA--GA AGG (-1)-3′
B2	5′-CTTGGAGCTGAAGAGGA--GA AGG (-1)-3′
C60	5′-CTTGGAGCTGAAGAGGA--GA AGG (-1)-3′

Biallelic mutation (*adf*)

WT	5′-CTTGGAGCTGAAGAGGAAGA AGG-3′
C66	5′-CTTGGAGCTGAAGAG---------- (-20)-3′
	5′-CTTGGAGCTGAAGAGGA--GA AGG (-1)-3′
C72	5′-CTTGGAGCTGAAGAG---------- (-53)-3′
	5′-CTTGGAGCTGAAGAGGA--GA AGG (-1)-3′

Heterozygous mutation (*adf*)

WT	5′-CTTGGAGCTGAAGAGGAAGA AGG-3′
J32	5′-CTTGGAGCTGAAGAGGAAGA AGG-3′
	5′-CTTGGAGCTGAAGAGGAGGA AGG-3′

(D)

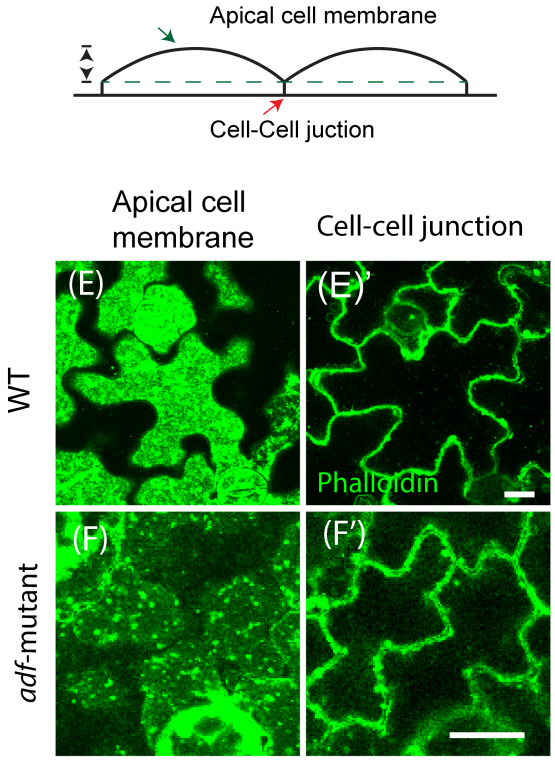

(G)

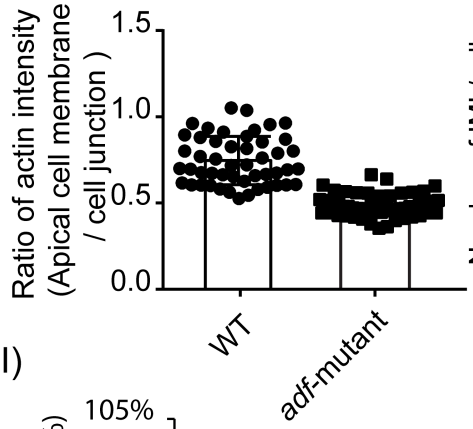

(H)

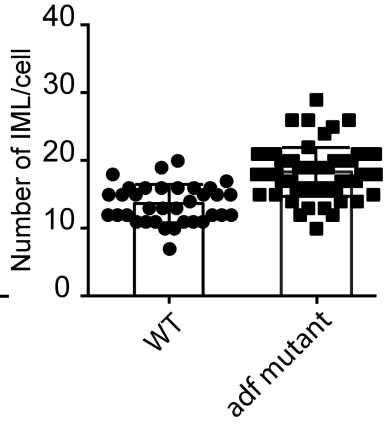

(I)

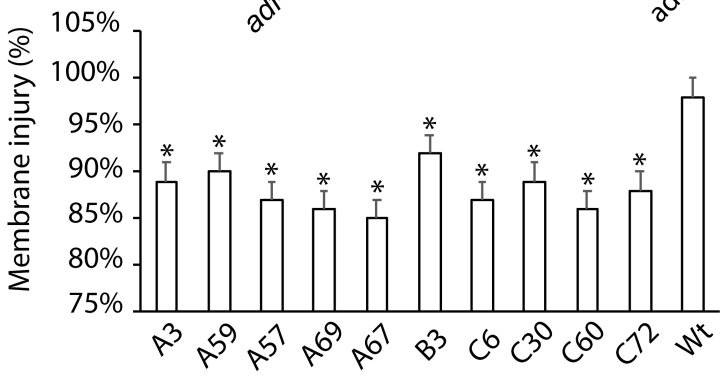

Figure 3

Analysis of RNP-mediated adf mutations in T0 plants. (A) Representative image showing the high-resolution melt analysis of an adf mutant (A57, red line) compared to wild-type (WT, blue line). (B) Representation of the adf gene mutation efficiency. (C) Sequence alignment of genome-edited mutants. (D) Schematic representation of the apical cell membrane and cell–cell junction. (E) Representative image of phalloidin-stained apical cell membrane Z projection in WT cells. (E') Representative image of phalloidin-stained cell-cell junction in WT cells. Scale bar = 20 μm. (F) Representative image of phalloidin-stained apical cell membrane Z projection in adf mutant A67. (F') Representative image of phalloidin stained cell–cell junction in adf mutant A67. Scale bar = 20 μm. (G) The ratio of actin intensity between the apical cell membrane and cell–cell junction in WT and adf mutant line A67 determined using ImageJ. Data are means ± SD (n = 3). The dots represent individual cells. (H) The number of IMLs from each cell. Data are means ± SD (n = 3). The dots represent individual cells. (I) Cell membrane thermostability measured using a conductivity meter under irrigated conditions in WT and adf mutant T0 plants. Data labelled with * show a significant difference in the cell membrane stability between mutants and wild-type plants, at $P \leq 0.05$, by Student's t-test. Data are means ± SD (n = 10).

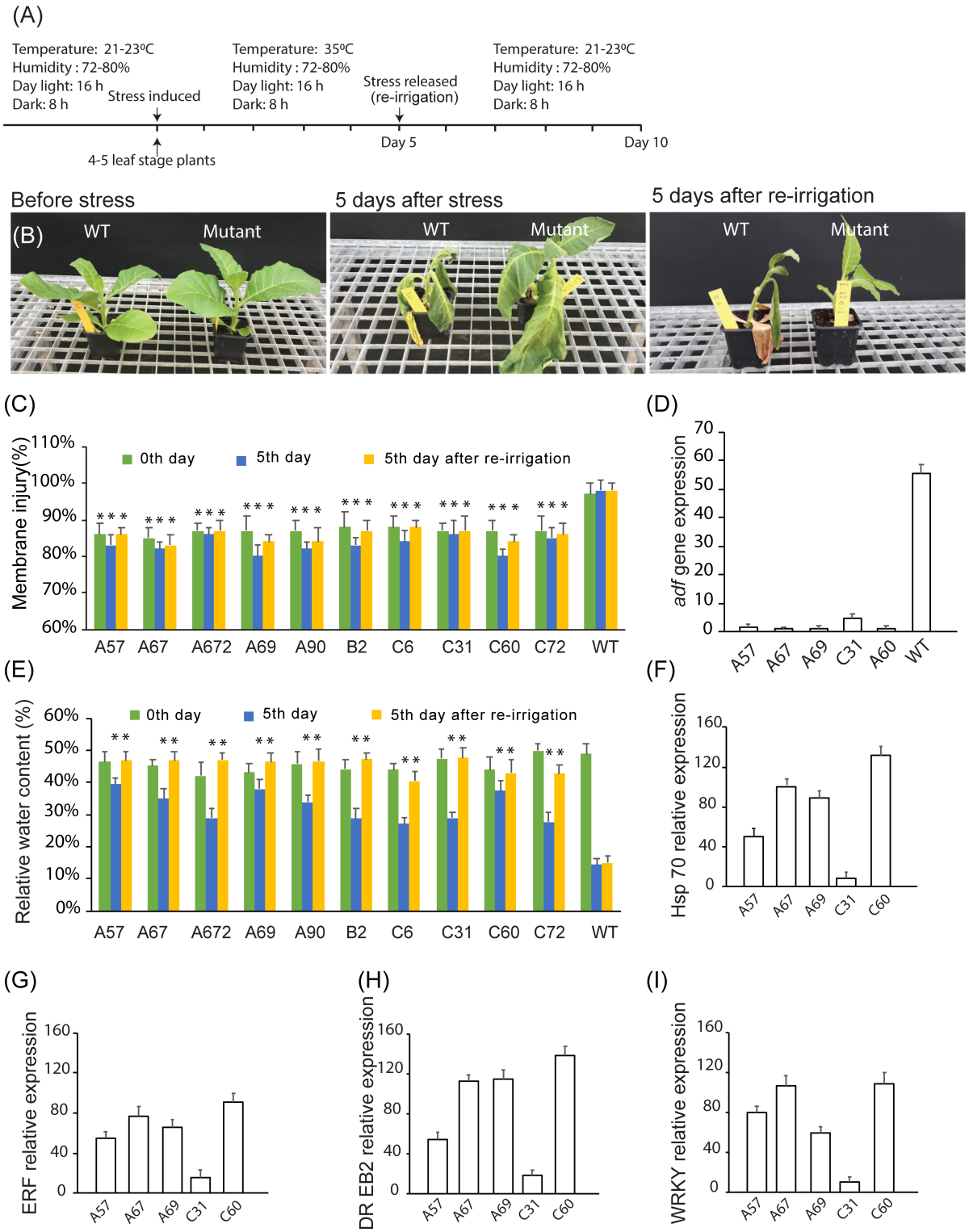

Figure 4

Analysis of drought stress tolerance in adf mutant T2 plants. (A) Schematic representation of the experimental timeline. (B) Representative images of wild-type (WT) and adf mutant plants on days 0 and 5 of drought stress and 5 days after the restoration of normal irrigation. (C) Membrane thermostability of the adf mutant and WT plants on days 0 and 5 of drought stress and 5 days after the restoration of normal irrigation. The data labelled with * show a significant difference in the CMS between mutants and

wild-type plants, at P ≤ 0.05, by Student's t-test. Data are means ± SD (n = 10). (D) Relative expression of adf in the adf mutants compared to WT plants under drought stress calculated using the comparative CT method. (E) Relative water content of the adf mutant and WT plants on days 0 and 5 of drought stress and 5 days after the restoration of normal irrigation. Data labelled with * shows a significant difference in the CMS between mutants and wild-type plants, at P ≤ 0.05, by Student's t-test. Data are means ± SD (n = 10). (F–I) Relative expression of stress-responsive genes in adf mutant plants (A57, A67, A69, C31 and C60) compared to WT under drought stress calculated using the comparative CT method: (F) Hsp70; (G) ERF; (H) DREB2; (I) WRKY. Data are means ± SD (n = 5).

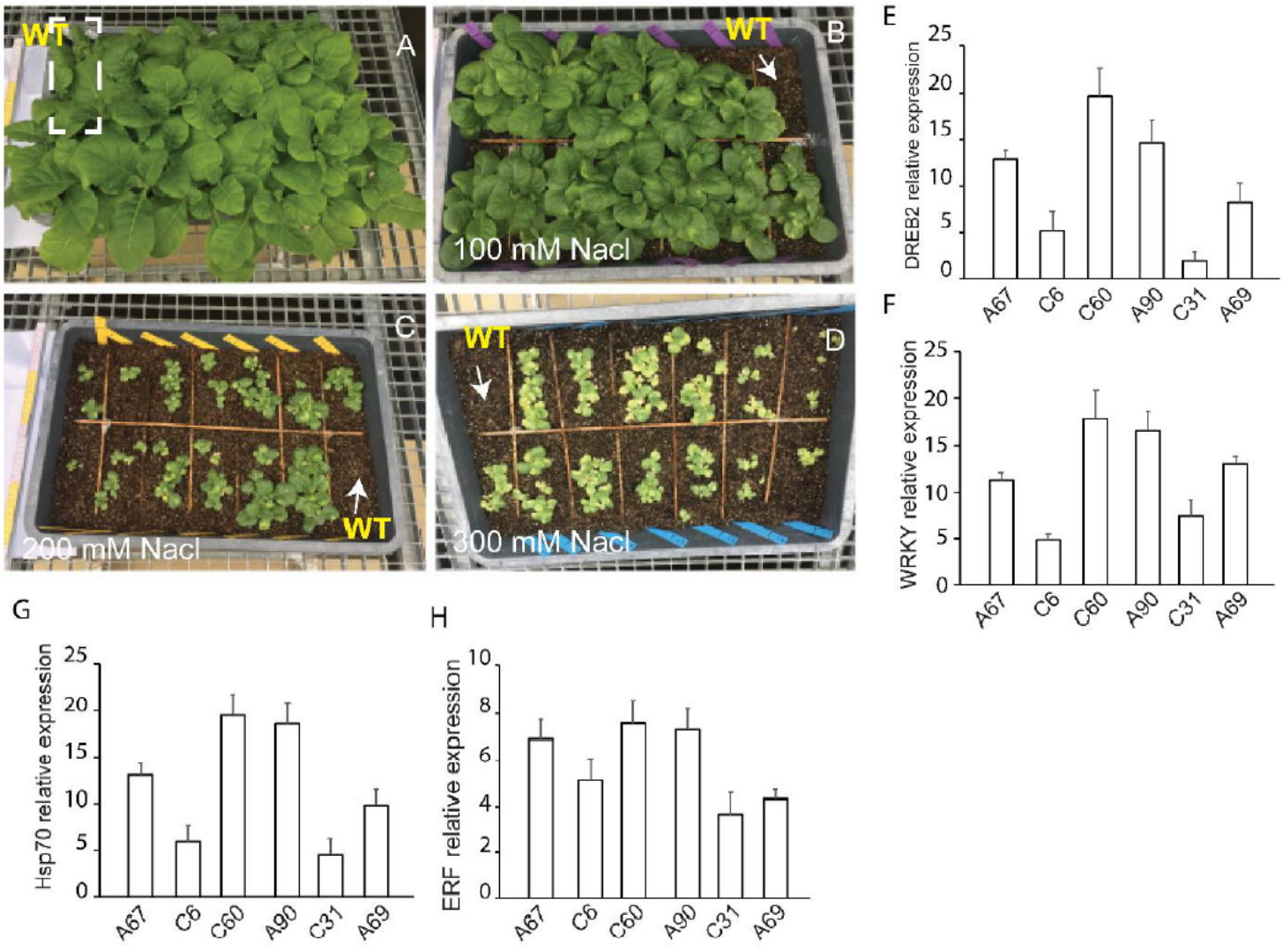

Figure 5

Analysis of salinity stress tolerance in adf mutant T2 plants. (A) Wild-type (WT) (white dotted area) and adf mutant plants at 0 mM NaCl. (B) WT (white arrow) and adf mutant plants at 100 mM NaCl. (C) WT (white arrow) and adf mutant plants at 200 mM NaCl. (D) WT (white arrow) and adf mutant plants at 300 mM NaCl. (E-H) Relative expression of stress-responsive genes in adf mutant plants (A67, C6, C60, A90, C31 and A69) compared to WT at 300 mM NaCl calculated using the comparative CT method: (E) DREB2; (F) WRKY; (G) Hsp70; (H) ERF. Data are means ± SD (n = 5).

Supplementary Files

This is a list of supplementary files associated with this preprint. Click to download.

- VideoS1.mov